Research Square

Preprints are preliminary reports that have not undergone peer review.
They should not be considered conclusive, used to inform clinical practice,
or referenced by the media as validated information.

Research on the Migration Patterns of Sand Dust in a Chongqing Foundry Company Based on Numerical Simulation

Jianwu Chen
University of Science and Technology Beijing
Xiyao Wu
University of Science and Technology Beijing
Fengqiong Chen
20181675@qq.com

Chongqing center for disease control and prevent
Ying Li
Chongqing center for disease control and prevent
Fabin Zeng
University of Science and Technology Beijing
Junjie Liu
University of Science and Technology Beijing
Guangyao Li
University of Science and Technology Beijing

Article

Keywords: sand dropping process, thermal plume, temperature difference buoyancy, CFD-DPM, dust migration

Posted Date: November 11th, 2026

DOI: https://doi.org/10.21203/rs.3.rs-11428251/v1

License: This work is licensed under a Creative Commons Attribution 4.0 International License.
Read Full License

Additional Declarations: No competing interests reported.

Research on the Migration Patterns of Sand Dust in a Chongqing Foundry Company Based on Numerical Simulation

Jianwu Chen[1,3], Xiyao Wu[1], Fengqiong Chen*[,2,3], Ying Li[2], Fabin Zeng[1], Junjie Liu[1], Guangyao Li[1]

1.State key Laboratory of Metal Mining Safety and Disaster Prevention and Control, University of Science and Technology Beijing, Beijing 100083, China

2.Chongqing center for disease control and prevent，choongqing，400707

3.NHC Key Laboratory for Engineering Control of Dust Hazard, University of Science and Technology Beijing, Beijing 100083, China

*Corresponding authors.Fengqiong Chen. Associate Chief Physician, 20181675@qq.com

Abstract: To clarify the impact of thermal plumes on the migration of casting sand dust, a semi-enclosed sand falling station at a foundry company in Chongqing was selected as the research object. On-site dust detection was conducted, and a CFD-DPM gas-solid two-phase flow model was established without applying The results indicate that the total dust concentration around the sand falling machine is 8.0-11.0 mg/m³, and there is significant dust pollution in the working area. As the high-temperature casting continues to cool, a vertical thermal plume gradually forms above the heat source. The peak velocity along the centerline increases from approximately 0.33 m/s at 1 second to about 0.49 m/s at 9 seconds. At 12 seconds, the peak remains relatively unchanged, but the high-speed region in the middle and upper parts continues to expand. The peak dust concentration is always located near the sand falling platform. As the thermal plume develops, the dust concentration in the middle and upper parts gradually increases, and the dust impact range continues to expand upward. In the later stages of the simulation, the

temperature field, velocity field, and dust concentration field within the Research indicates that the upward airflow generated by thermal buoyancy plays a crucial role in the vertical migration of falling dust. The area above the heat source and the deflection zone at the top of the equipment are key positions that require focused attention for dust control.

Keywords: sand dropping process; thermal plume; temperature difference buoyancy; CFD-DPM; dust migration

1. Introduction

The foundry industry is an important foundational sector of the machinery manufacturing industry, and shakeout is the key process for separating castings from molding sand and sand cores. During the sand falling process, accompanied by strong mechanical disturbances such as vibrations and impacts, as well as the influence of thermal plumes, a large amount of dust is generated, severely endangering the occupational health of workers. Therefore, revealing the spatiotemporal migration characteristics of sand dust under the influence of thermal plumes can provide technical guidance for the engineering protection against sand dust hazards.

In recent years, scholars both domestically and internationally have conducted extensive research on occupational exposure to foundry dust, the migration characteristics of particulate matter, and numerical simulation methods. Siltanen E et al. [1] investigated the dust exposure in Finnish foundries, revealing the prevalence of dust exposure in the foundry work environment; Andersson L et al. [2] analyzed the characteristics of quartz and dust exposure in Swedish iron foundries, pointing out that dust and quartz-containing particulate matter during the casting process are significant factors affecting the occupational health of workers. On this basis, Tong R et al. [3] established a quantitative health risk assessment method for inhalation exposure to

automotive casting dust, Duan D et al. [4] analyzed the occupational exposure risks of dust and noise in iron foundries in China, and Li Q et al. [5] further compared the applicability of various risk assessment methods in positions with excessive dust concentrations in iron foundries. The above studies show that exposure to casting dust has a prominent occupational health risk, and its degree of harm is closely related to dust concentration, particle properties and spatial distribution. The research of Gong X et al. [6] shows that particle size is an important factor affecting the movement and separation behavior of casting dust. In the research of industrial dust transportation, numerical methods such as CFD and discrete phase model have been widely used. Cai Y et al. [7] analyzed the transport and diffusion characteristics of dust under single and coupled dust source conditions, revealing the impact of interactions between different dust sources on the spatial distribution of dust. Huo S et al. [8] studied the effect of changes in mining intensity on dust distribution characteristics. Xue S et al. [9] analyzed the movement patterns of dust during the mining process from the perspectives of Li Y et al. [10] studied the distribution patterns of airflow and dust under multi-process operating conditions, indicating a close relationship between the airflow structure and dust transport in complex operational spaces. In open or semi-open spaces, the external environment and spatial structure will also alter the dust dispersion process. Tian D et al. [11] studied the dust distribution patterns under different depth conditions in open-pit coal mines; Zhou W et al. [12] analyzed the diffusion characteristics of dust from transport vehicles under vertical wind shear; Wang Z et al. [13] used the WRF-FLUENT coupling method to simulate the airflow and dust diffusion process in open-pit mines in cold regions; Wang J et al. [14] further investigated the distribution and Tang S et al. [15], in their review of the movement patterns and numerical simulation studies of coal mine dust, pointed out that the transport

behavior of dust under complex airflow conditions is influenced by multiple factors, including the dust generation process, particle properties, and the environmental flow field. An J et al. [16] combined CFD-DPM simulation with individual monitoring to analyze the exposure mechanisms of inhalable dust; Yu H et al. [17] studied the migration and deposition characteristics of fine particulate matter from the perspective of the human upper respiratory tract, further indicating that dust migration research can extend from the transport in the work environment to the scale of human exposure. Generally speaking, the existing research has achieved more results in dust occupational exposure, particulate transportation and numerical simulation, but the research objects are mainly concentrated in typical high-dust environments such as coal mines, open-pit mines and tunnels, and the research on the casting sand falling process is still relatively limited. In particular, there is still a lack of systematic research on how the hot plume formed by high-temperature castings and residual sand absorbs and transports dust, and how dust gradually develops from near-source aggregation to vertical elevation, lateral deflection and spatial diffusion; the space-temporal correspondence between temperature field, velocity field and dust concentration field and its inherent mechanism of action are also to be studied. Further reveal.

Based on this, this paper takes the sand falling process of a foundry enterprise in Chongqing as the research object, grasps the sand falling process, equipment structure and operating space characteristics through on-site investigation, and establishes a three-dimensional calculation model according to the actual sand falling equipment and operation area. Using the method of combining computational fluid dynamics and discrete phase model, a numerical model of CFD-DPM gas-solid two-phase flow considering the buoyancy effect of temperature difference is constructed, and the transient evolution of temperature field, velocity field and dust concentration field in the

process of sand falling without mechanical ventilation is simulated. By analyzing the changes in the spatial distribution of dust during the formation, development and deflection of thermal plumer flow, the absorption, lifting and diffusion behavior of dust driven by thermal buoyancy are studied, and the phased transport path of falling sand dust released from the near source to the upper space diffusion is summarized. The research results can provide a theoretical basis for the identification of high-risk areas of dust in the casting process and the reasonable arrangement of subsequent dust-proof and dust removal facilities.

2.Overview of the Research Subject

2.1 Sand Falling Process and Dust Generation Characteristics

The sand casting process mainly includes molding, core making, boxing, smelting and pouring, cooling and solidification, sand falling, cleaning and inspection and other links. Shakeout is carried out after the casting has cooled and solidified and before its surface is cleaned. This step separates the casting from the molding sand and sand core. Once pouring is complete and the casting has cooled sufficiently, the flask is transported to the shakeout area. The sand mold and core are then broken apart by opening and turning the flask, together with mechanical vibration and impact, so that the casting can be separated from the sand. The separated waste sand falls through the openings in the shakeout screen and enters the collection and conveying system below, while the casting is transferred to the next cleaning stage. Fig. 1 shows the workflow of the shakeout process.

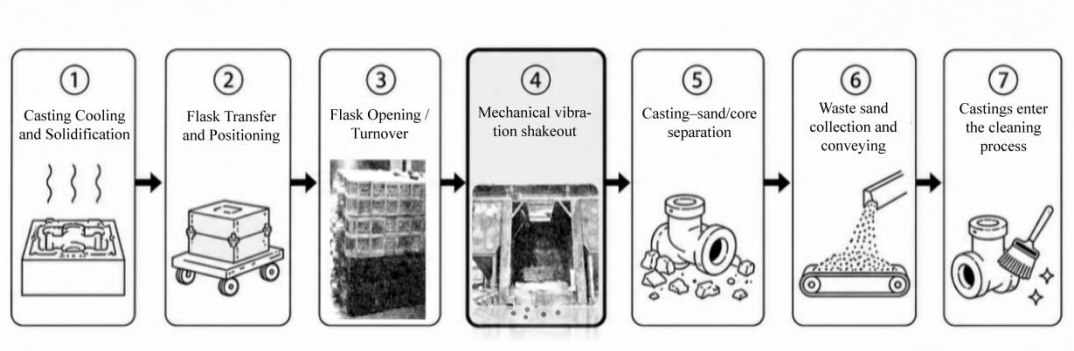


Fig. 1. Sand Casting Process Flowchart

It can be seen from Fig. 1 that mechanical vibration falling sand is the core link of sand mold crushing and casting separation from mold sand, and it is also the main stage of concentrated dust release. During the sand-dropping operation, the sand mold and sand core are gradually broken under the action of vibration, impact and flipping, and collision and friction continue to occur between the sand blocks, castings and equipment. The fine powder on the surface of the sand, the sand core debris and the residual particles attached to the surface of the casting are peeled off under mechanical action, and enter the surrounding air with the falling of waste sand and the vibration of the equipment, forming an obvious instantaneous and intermittent dust release process. Therefore, the mechanical vibration sand falling stage is the focus of analyzing the characteristics of dust generation and initial migration.

This article takes the sand falling process of a foundry enterprise in Chongqing as the research object. Its sand falling operation area adopts a semi-closed structure, which is mainly composed of the main body of the sand dropping machine, the sand falling platform, the sandbox transfer area and the enclosure structure on both sides. The spatial arrangement is shown in Figure 2. The sand dropper is set up in the fixed workstation of the workshop. The sandbox or mold is sent to the operation area through the front transshipment device. After the positioning is

completed, the box is opened, the box is turned over and the sand is mechanically vibrated in turn. According to on-site surveying and mapping, the width of the front opening of the sand-dropping machine is about 5790 mm, the internal effective operation width is about 4,620 mm, the width of the sand-dropping platform is about 4160 mm, and the internal height of the equipment is about 4850 mm. The falling sand platform is located at the bottom of the equipment, which is the main area for sand crushing, casting separation and dust release.



Fig. 2. Diagram of the Sand Drop Work Area and Existing Ventilation Facilities

It can be seen from Fig. 2 that the sand-dropped workstion adopts a semi-closed structure, with an enclosure structure on both sides, and a large opening at the front to meet the needs of sandbox transshipment and personnel operation. There are jet air curtains, left and right exhaust ports and top exhaust outlets on the site. The internal space of the equipment, the front opening and the upper area are connected to each other, and the enclosure structure and the opening position together form the spatial boundary of the migration of dust-containing airflow. It should be noted that Figure 2 is used to show the actual structure and ventilation facilities of the sand-falling workstation. In order to study the impact of temperature difference buoyancy on dust migration separately, the subsequent numerical simulation does not apply mechanical air supply

and exhaust, and only the geometric characteristics such as the main body of the equipment, the enclosure structure and the main opening are retained.

Judging from the dust production process, the formation of falling sand dust mainly includes three aspects: sand type crushing, particle peeling and waste sand secondary dust. First of all, water loss, embrittlement and local sintering may occur in the process of high-temperature pouring and cooling, causing the bonding state between the sand particles to change; under the action of mechanical vibration and impact, the sand mold and sand core structure are rapidly broken and fine particles are released. Secondly, the collision and friction between the sand block, the casting and the equipment make the fine powder attached to the sand grain and the surface of the casting constantly peel off and enter the air. Finally, the crushed waste sand is continuously disturbed during falling, screening and conveying, and the sedimented particles may be raised again, thus prolonging the suspension and diffusion time of dust in the operating space.

The particles produced by mechanical crushing and peeling have different motion characteristics. Larger particles are strongly affected by gravity and inertia. After release, they usually move near the dust source and settle faster; particles with smaller particle size have a lower sedimentation rate and strong airflow followability, and are easier to migrate to the upper part of the equipment and the surrounding operating space with the local airflow. Continuous vibration, waste sand drop and equipment collision during sand falling may also cause the sedimented particles to rise for the second time, causing the dust to change dynamically between near-source release and spatial diffusion.

In addition to mechanical disturbance, the thermal environment formed by high-temperature castings and residual sand is also an important factor affecting the migration of dust. During the

operation of falling sand, the temperature of the casting and the mold sand is usually higher than the temperature of the surrounding air. The temperature difference between the two reduces the density of the adjacent air after being heated and moves upwards, gradually forming a hot plumer flow. After the dust generated by mechanical action enters the hot plumer flow, it is sucked and transported upwards under the action of airflow drag, so that the dust migrates from the near-source area near the falling sand platform to the upper part of the equipment. With the continuous development of hot plume, its flow direction may also be deflected by the influence of equipment enclosure structure, open boundaries and local backflow, thus driving dust to spread to the lateral and front working space.

In summary, the generation and migration of falling sand dust is the result of the joint action of mechanical disturbance, particle force, thermal buoyancy and spatial boundaries. Sand crushing, particle peeling and waste sand disturbance determine the release position and initial movement state of the dust. The hot plume formed by high-temperature castings and residual sand further drive the dust upward transport and may cause lateral deflection in the upper part of the equipment. As a result, falling sand dust presents a basic migration process of "near source release - hot plumer coil suction - vertical lifting - lateral diffusion". In the future, a numerical model will be established according to the actual spatial structure of the falling sand operation area, further analyze the transient evolution characteristics of the temperature field, velocity field and dust concentration field, and reveal the space-time movement law of falling sand dust by the action of hot plumer flow.

2.2 Analysis of Dust Characteristics and On-Site Concentration Measurement

In order to understand the falling sand dust from the two levels of particle characteristics and on-site pollution level, and to provide a basis for subsequent CFD-DPM numerical simulation, this paper first characterizes the particle size distribution and micromorphology of the collected dust, analyzes the suspension, settlement and flow migration potential of different particles; and then determines the total powder in the sand falling operation area. Dust mass concentration, evaluate the degree of dust pollution and spatial differences under actual operation conditions. Among them, the particle size directly affects the inertial response, gravity sedimentation and tracking ability of dust in the airflow, which is an important basis for the particle size setting of the DPM model; the micromorphology can assist in judging the irregularity and aggregation characteristics of particles; the on-site concentration determination reflects the actual pollution after the joint action of dust production, sedimentation and airflow transportation Result.

Using a laser particle size analyzer to test the particle size of the falling sand dust, the results are shown in Fig. 3.

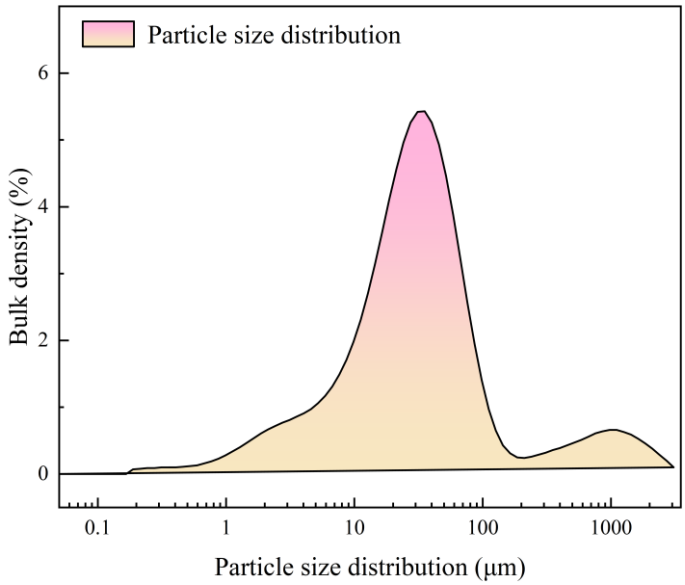
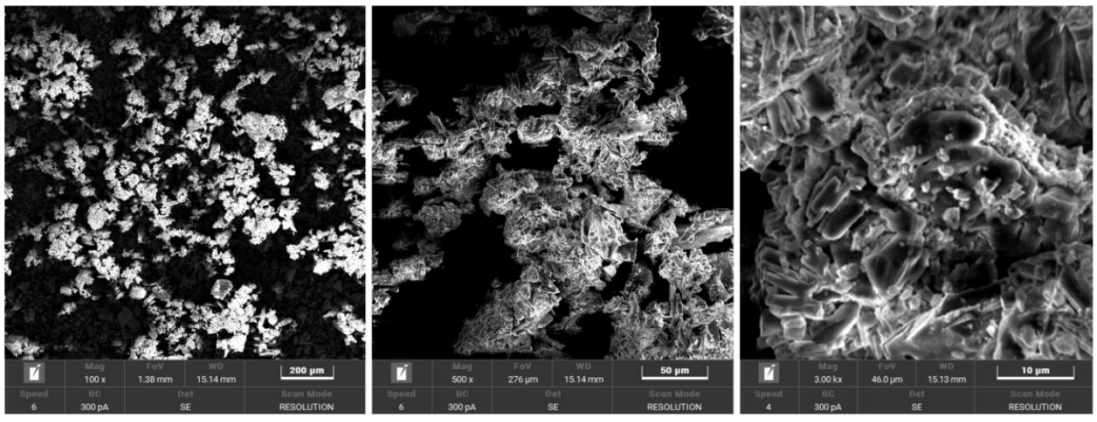


Fig. 3. Particle Size Distribution Curve

As shown in Fig. 3, the particle size distribution of the falling sand dust is quite broad, with the particle volume distribution mainly concentrated around 20-70 μm. The Dv(10), Dv(50), and Dv(90) are 5.263, 31.640, and 172.440 μm, respectively, indicating the coexistence of Among them, fine particles smaller than 10 μm have weaker settling ability and stronger airflow following, making them more likely to be suspended and migrate toward the upper part of the equipment under the influence of thermal plumes; larger particles are more significantly affected by inertia and gravity, and after being released, they tend to move and settle near the dust generation Therefore, the particle size distribution not only reflects the multi-scale characteristics of the dust but also provides a basis for determining the particle size range in subsequent simulations and explaining the migration differences of particles of different sizes.

To further identify the particle morphology and agglomeration state of the fallen sand dust, the collected dust samples were observed using a scanning electron microscope, as shown in Fig. 4.



(a) Overall distribution at low magnification (b) Typical particle morphology (c) Fine particles and agglomeration features in selected regions

Fig. 4. SEM Morphology of Sand Dust

It can be seen from Fig. 4 that the whole falling sand dust particles are irregular block-shaped, flake-shaped and flocculent, with a rough surface, and pores, folds and cracks can be seen; some

small particles are attached to the surface of larger particles, and there is obvious aggregation in some places. This shape coincides with dust-producing processes such as sand crushing, friction peeling and particle collision, which also indicates that the airflow response of actual dust may be affected by particle irregularity and aggregation state. Combined with the particle size results, it can be seen that the falling sand dust has the characteristics of multi-scale particle size and irregular morphology, and there may be differences in the suspension, sedimentation and migration ability of different particles in the airflow. The above characterization reveals the migration potential of dust, but it cannot directly explain the degree of pollution in the actual operation area. Therefore, it is necessary to further evaluate the dust pollution level and spatial differences of the sand falling site in combination with the on-site dust concentration measurement.

To understand the pollution levels of the aforementioned particles under actual sand dropping operation conditions, this paper measures the total dust mass concentration in the operation area. The detection was conducted in accordance with the "Standard for Determination of Dust in the Air of Workplaces Part 1: Total Dust Concentration" (GBZ/T 192.1—2025), using the filter membrane weighing method to measure the total dust concentration in the air of the sand dropping operation area. The calculation equation is:

$$C = \frac{(m_2 - m_1) \times 1000}{V} \quad \text{(Equation.1)}$$

In the equation:

C is the total dust concentration, mg/m³;

m_1 is the mass of the filter membrane before sampling, mg;

m_2 is the mass of the filter membrane after sampling, mg;

240 V is the volume of air sampled under standard conditions, L.

241 **Table 1.** Total Dust Concentration Measurement Results in the Sandfall Operation Area

Detection area	Total dust concentration (mg/m³)
The area around the sand drop machine	8.0-11.0
Peak value of the operating position	10.7
Work area forward detection point	9.2

242 As shown in Table 1, the total dust concentration in the area around the sand drop machine is
243 8.0-11.0 mg/m³, with the peak concentration at the operator's position being 10.7 mg/m³ and the
244 concentration at the forward detection point in the work area being 9.2 mg/m³. Each detection
245 location is at a relatively high concentration level, indicating that there is significant dust pollution
246 in the sand falling operation area; the differences in concentration between different locations
247 suggest that the dust is not evenly distributed within the operational space. Combining the
248 characterization results of Figures 3 and 4, the sand dust contains both larger particles that easily
249 settle in the near-source area and finer particles with strong transportability. The multi-scale
250 particle size distribution and irregular, agglomerated morphology may jointly influence the dust
251 suspension and sedimentation distribution at different locations.

252 Based on the characteristics of dust and the results of on-site concentration, the mechanical
253 crushing, particle detachment, waste sand drop, and equipment vibration near the sand falling
254 platform constitute the main dust release processes. After release, larger particles are more likely
255 to settle in the near-source area due to the effects of gravity The difference in particle size
256 determines the migration potential of the dust, while the spatial difference in on-site concentration
257 reflects the result of the combined effects of dust generation, sedimentation, thermal buoyancy,

and equipment boundaries. Therefore, relying solely on concentration measurement points makes it difficult to explain the continuous process of dust release from the source to its diffusion upwards; further analysis is needed in conjunction with the flow field and particle movement.

Based on the above understanding, the subsequent numerical simulation will take the actual measurement of particle size distribution as the basis for setting particle parameters, and combine the structure of the falling sand equipment and the heat source conditions. Through the transient evolution of temperature field, velocity field and dust concentration field, the process of coiling, lifting and diffusion of particles of different particle sizes under the action of thermal plumer flow will be studied, so as to explain the spatial concentration difference reflected by the on-site detection point and its possible formation mechanism.

It should be noted that there are differences between on-site testing and subsequent numerical simulation in terms of ventilation status, dust release intensity and time scale. On-site testing is used to characterize the pollution level and spatial differences in the actual sand-falling operation area. Particle size and morphology characterization are used to support particle parameter selection and migration mechanism interpretation. The two together constitute the on-site basis for numerical model establishment and result analysis, but not used to verify the absolute value of simulated concentration. The follow-up simulation focuses on the relative distribution, main migration path and dynamic evolution law of the dust concentration field under given release conditions.

3 Establishment and Methods of Numerical Models

3.1 Mathematical Model of Gas-Solid Two-Phase Flow

During the shakeout process, mechanical vibration, impact, and sand-mold breakage release

dust into the surrounding air. The dust is then transported under the combined effects of airflow drag, gravity, and thermal buoyancy. This process is a typical gas-solid two-phase flow, where the air medium is considered the continuous phase and the dust particles are considered the discrete phase. This paper employs a method that combines computational fluid dynamics with a discrete phase model to numerically solve the airflow and dust particle movement in the sand dropping operation area.

The air velocity in the sand dropping operation area is relatively low, allowing the air to be considered as an incompressible fluid. The continuous phase airflow satisfies the mass conservation equation and the momentum conservation equation. Respectively expressed as:

$$\nabla \cdot u = 0 \qquad \text{(Equation.2)}$$

$$\rho\left(\frac{\partial u}{\partial t} + u \cdot \nabla u\right) = -\nabla p + \nabla \cdot \left[\mu\left(\nabla u + \nabla u^{T}\right)\right] + \rho g + F_b \qquad \text{(Equation.3)}$$

In the equation:

u is the velocity vector of the continuous phase, m/s;

ρ is the air density, kg/m³;

p is the fluid pressure, Pa;

μ is the air dynamic viscosity, Pa·s;

g is the gravitational acceleration, taken as 9.81 m/s²;

F_b is the buoyancy source term caused by temperature difference, N/m³.

During the sand falling operation, there is a significant temperature difference between the high-temperature castings and residual sand and the surrounding air. The adjacent air, after being heated, undergoes a change in density and forms an upward-moving thermal plume under the influence of buoyancy.To account for the effects of thermal plumes on airflow structure and

dust-transport pathways, both gravity and thermal buoyancy are included in the continuous-phase momentum equation. The energy equation is also enabled during the simulation, while temperature-induced variations in air density are described using the Boussinesq approximation. The heat-source conditions and other simulation parameters are provided in the boundary conditions section.

The motion of dust particles in the airflow is described using the Lagrangian method, and the particle motion equation is established based on Newton's second law. According to the numerical model actually used in this paper, the motion of particles mainly considers the effects of aerodynamic drag, gravity, and buoyancy, and its motion equation is:

$$\frac{du_p}{dt} = \frac{18\mu}{\rho_p d_p^2} \cdot \frac{C_D \,\mathrm{Re}_p}{24}\left(u - u_p\right) + \frac{\rho_p - \rho}{\rho_p} g \qquad \text{(Equation.4)}$$

In the equation:

u_p is the particle velocity vector, m/s;

u is the continuous phase airflow velocity vector, m/s;

ρ_p is the particle density, kg/m³;

ρ is the air density, kg/m³;

d_p is the particle diameter, m;

μ is the air dynamic viscosity, Pa·s;

C_D is the particle drag coefficient, dimensionless;

Re_p is the particle relative Reynolds number, defined as $\mathrm{Re}_p = \frac{\rho d_p \left|u - u_p\right|}{\mu}$, dimensionless;

g is the gravitational acceleration vector, taken as 9.81 m/s².

The first term on the right side of Equation 4 is the aerodynamic resistance term generated by the relative motion between the airflow and the dust particles, and the second term is the body force term formed by the combined action of gravity and buoyancy. Aerodynamic drag causes dust particles to tend to move with the surrounding airflow, while gravity and buoyancy influence the vertical movement and settling process of the particles. Particles of different sizes have varying inertia and airflow following capabilities, so their migration and sedimentation behavior in thermal plumes will also differ.

This paper mainly studies the impact of thermal plumes on the migration paths of sediment dust at the operational space scale, while keeping the mathematical model consistent with the actual numerical solution settings. The forces acting on the particles only consider aerodynamic drag, gravity, and buoyancy, without introducing additional effects such as Brownian force For the sparse-phase dust transport process studied in this paper, considering the low mass flow rate of the particle phase and the small particle volume fraction, the reverse effect of the particles on the continuous phase flow field is relatively limited. Therefore, a one-way coupling method is used for calculations, where the continuous phase airflow

Airflow within the sand-shakeout zone is influenced by factors such as the main equipment body, the shakeout platform, enclosures, and open boundaries; phenomena such as rising thermal plumes, near-wall flow, and local recirculation are present, resulting in a flow field characterized by complex turbulence. In this study, the SST k-ω turbulence model is employed to describe the turbulent flow of the continuous phase.This model combines the advantages of the k-ε model near walls with those of the k-ε model in free-stream regions. It is therefore well suited to simulating flow fields with adverse pressure gradients, flow separation, and complex recirculating airflow.

The general forms of the transport equations for turbulent kinetic energy k and specific dissipation rate ω in this model are as follows:

$$\frac{\partial(\rho k)}{\partial t}+\frac{\partial(\rho k u_j)}{\partial x_j}=P_k-\beta^*\rho k\omega+\frac{\partial}{\partial x_j}\left[(\mu+\sigma_k\mu_t)\frac{\partial k}{\partial x_j}\right] \quad \text{(Equation.5)}$$

$$\frac{\partial(\rho\omega)}{\partial t}+\frac{\partial(\rho\omega u_j)}{\partial x_j}=\alpha\frac{\omega}{k}P_k-\beta\rho\omega^2+\frac{\partial}{\partial x_j}\left[(\mu+\sigma_\omega\mu_t)\frac{\partial\omega}{\partial x_j}\right]+D_\omega \quad \text{(Equation.6)}$$

In the equation:

k is the turbulent kinetic energy, m^2/s^2;

ω is the specific dissipation rate, rad/s;

ρ is the air density, kg/m^3;

t is time, s;

u_j is the velocity component of the airflow, m/s;

P_k is the generation term for turbulent kinetic energy, $kg/(m\cdot s^3)$;

β^* is a model constant;

μ is the dynamic viscosity of air, Pa·s;

σ_k is the turbulent Prandtl number for turbulent kinetic energy;

μ_t is the turbulent viscosity, Pa·s;

α is a model constant;

β is a model constant;

σ_ω is the turbulent Prandtl number for the specific dissipation rate;

D_ω is the cross-diffusion term, $kg/(m\cdot s^3)$, defined as $D_\omega=2(1-F_1)\rho\sigma_{\omega^2}\frac{1}{\omega}\frac{\partial k}{\partial x_j}\frac{\partial\omega}{\partial x_j}$;

F_1 is the first blending function, used to achieve a smooth transition between models $k-\omega$ and $k-\varepsilon$.

In summary, this paper describes the airflow in the sand falling operation area using the incompressible continuous phase control equation. It reflects the thermal plume effect caused by high-temperature castings and residual sand through the temperature difference buoyancy source term and energy equation. The SST k-ω model is used to describe the complex turbulent structure, and the discrete phase The aforementioned mathematical model provides a computational basis for the subsequent analysis of the transient evolution of the temperature field, velocity field, and dust concentration field.

3.2 Geometric Model and Mesh Generation

Based on the on-site layout, equipment dimensions, and spatial structural characteristics of the sand falling process at a foundry in Chongqing, a three-dimensional geometric model of the sand falling operation area was established using SolidWorks software. The model is based on the on-site sand drop machine and its surrounding operational space, primarily retaining the main body of the sand drop machine, the sand drop platform, the equipment enclosure structure, the main openings, and the dust release area, in order to reflect the main spatial boundaries involved in the formation of thermal The positions of the on-site jet air curtain and the left, right, and top exhaust openings are considered in the geometric structure, but mechanical ventilation or suction is not applied during the calculations to eliminate the interference of active ventilation on the flow field, allowing for a separate analysis of the dust migration process driven by thermal The 3D model of the sand dropper is shown in Fig. 5.

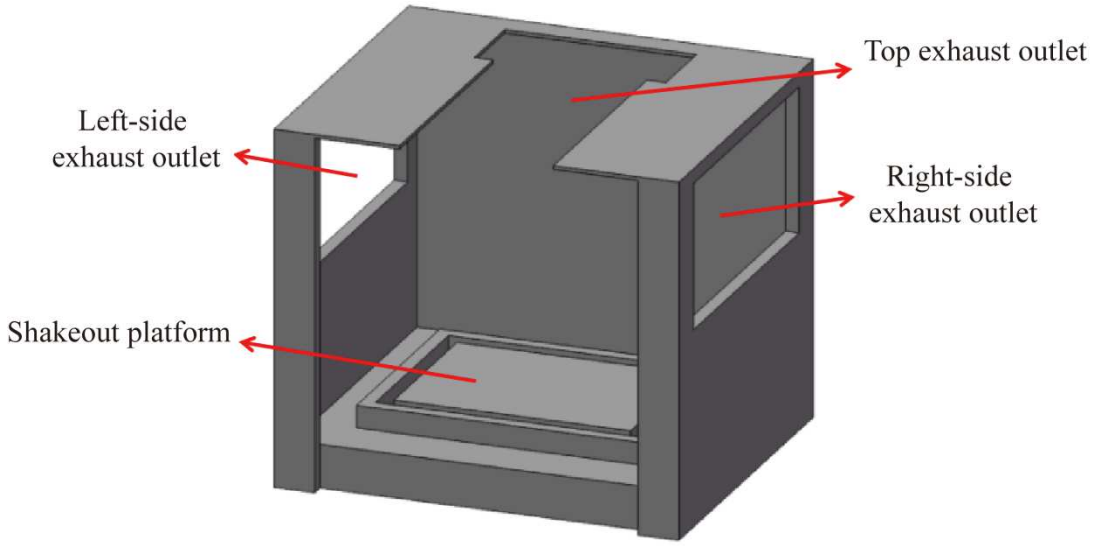
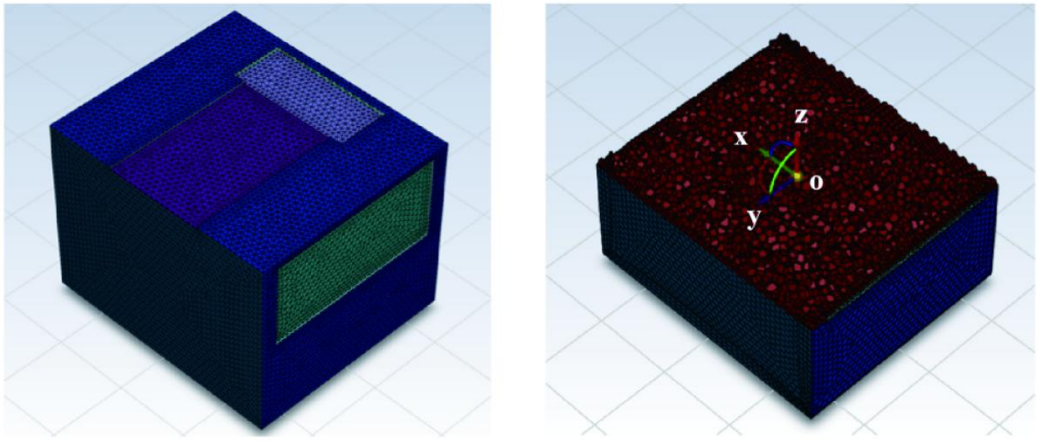


Fig. 5. 3D Model of the Sand Drop Machine

To improve the computational efficiency of numerical simulations, the actual equipment was appropriately simplified without altering the main structure and primary flow space of the sand dropping operation area. During the modeling process, local structures such as bolts, chamfers, and small holes, which have a minimal impact on the overall flow field, were ignored. The main body shape of the sand dropper, the sand drop platform, the enclosure structure, the main openings, and the dust release areas were retained The simplified model can reflect the impact of heat source location, dust release location, and equipment boundaries on the development of thermal plumes and the spatial migration of dust, while avoiding the increase in mesh count and computational cost caused by excessive small structures.

After completing the 3D geometric model, Fluent Meshing is used to mesh the computational domain, and the mesh and its profile in the sand dropping operation area are shown in Fig. 6. The model employs a structured hexahedral mesh to achieve a reasonable balance between computational accuracy and efficiency.



(a) Schematic of the computational mesh (b) Mesh cross section

400

401 Fig. 6. Schematic Diagram and Sectional View of the Grid Division in the Sand Falling Workshop

402 In the process of grid division, local encryption is carried out in areas with obvious changes
403 in the convection field and concentrated dust migration to improve the analysis ability of thermal
404 plume development, local return flow and dust concentration gradient. A three-layer boundary
405 layer grid is set up near the ground, the sand-falling equipment wall and the workshop enclosure
406 structure. The growth rate of the boundary layer is 1.999, and the height of the first layer is 17.99
407 mm, which is used to improve the numerical analysis of the airflow movement and particle
408 settlement process in the near-wall area.

409 In order to evaluate the quality of the grid, the divided grid is checked, and the orthogonal
410 quality is taken as the main evaluation indicator. The closer the orthogonal mass value is to 1, the
411 more regular the grid unit form is. According to statistics, the maximum value of the orthogonal
412 mass of the model grid is 0.9999, the average value is 0.858, and the minimum value is 0.19. The
413 average orthogonal quality of the overall grid is relatively high, and the minimum orthogonal mass
414 is also higher than the lower limit of 0.05 judgment adopted by the original model, indicating that
415 the quality of the grid unit meets the subsequent numerical solution requirements.

416 In order to reduce the impact of the number of grids on the calculation results, different

numbers of grids are used for comparative calculations while maintaining the same geometric model, boundary conditions and solution parameters. Considering that this paper needs to analyze the process of dust migration from near the falling sand platform to the operating space, the average dust mass concentration of the horizontal cross-section at a height of 1.5 m above the ground is selected as the grid independence evaluation index. The calculation results under the number of different grids are shown in Fig. 7.

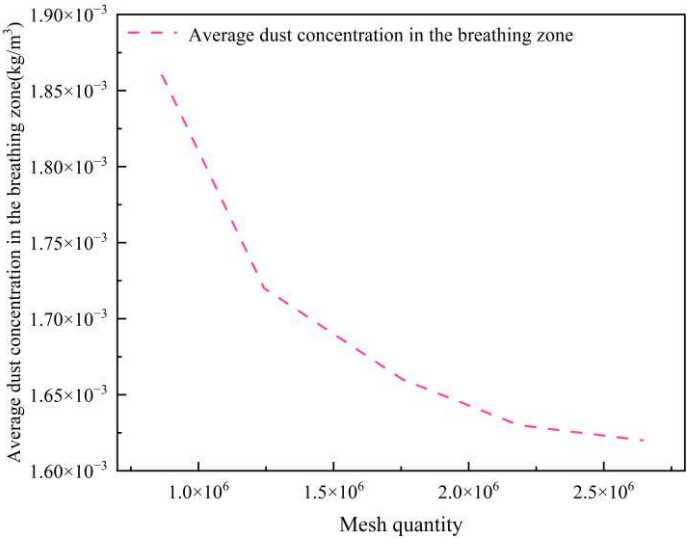


Fig. 7. Grid Independence Analysis Chart

As shown in Fig. 7, as the number of grids increases from 8.65×10^5 to 2.64×10^6, the average dust mass concentration at a horizontal section 1.5 m above the ground gradually stabilizes. When the number of grid cells reaches 2.19×10^6, further increasing the number of grid cells results in a change rate of less than 5% in the calculation results, indicating that further refining the grid has a minimal impact on the average dust concentration at this section. Considering both the computational accuracy and the computational cost, approximately 2.19×10^6 grid cells were ultimately selected for subsequent transient numerical simulations.

In summary, this paper establishes a three-dimensional geometric model based on the on-site sand dropping equipment and the working space. Through local mesh refinement, boundary layer

settings in the near-wall region, mesh quality checks, and mesh independence analysis, approximately 2.19×10^6 mesh elements are determined as the This mesh can meet the numerical analysis requirements for the development of thermal plumes, airflow movement in the working space, and dust migration processes.

3.3 Boundary Conditions and Particle Parameters

To separate the effects of mechanical ventilation and thermal buoyancy, this paper establishes a baseline condition without mechanical supply and exhaust ventilation, focusing on revealing the natural migration patterns of falling dust particles under thermal effects only. This operating condition does not fully replicate the actual operating state of the on-site ventilation system but is used to identify the basic path of thermal plume formation, development, and its dust-carrying migration. The continuous phase uses a pressure-based transient solver, with velocity expressed as absolute velocity, turbulence modeled with the SST $k-\omega$ model, and pressure-velocity coupling using the SIMPLE algorithm. During the calculation process, the gravity and energy equations are enabled, and the Boussinesq hypothesis is used to describe the changes in air density caused by temperature differences.

The surface temperature of the high-temperature casting is set to 180 ℃, and the initial ambient temperature is set to 25 ℃. The supply air boundary velocity corresponding to the on-site air curtain is set to 0 m/s, and no mechanical suction is applied to the left, right, and top exhaust outlets, treating them as open boundaries. The initial velocity in the computational domain is set to 0 m/s, so the airflow within the computational domain is primarily driven by the temperature difference between the high-temperature surface and the surrounding air. Through this setup, the mechanical supply and exhaust can be avoided from altering the thermal plume structure, thereby

identifying the independent effects of thermal buoyancy on dust entrainment, vertical transport, and lateral diffusion. The transient simulation duration is 15 seconds, and characteristic moments are selected at 1.0, 5.0, 9.0, and 12.0 seconds to analyze the evolution process of the thermal plume and dust concentration field. The continuous phase boundary conditions and solution settings are shown in Table 2.

Table 2. Continuous Phase Boundary Conditions and Solution Settings

Parameter	Setting
Solver	Pressure-based solver
Simulation type	Transient
Velocity formulation	Absolute velocity formulation
Turbulence model	SST $k-\omega$
Pressure–velocity coupling scheme	SIMPLE
Energy equation	Enabled
Gravitational acceleration	9.8 $m \cdot s^{-2}$
Density model	Boussinesq approximation
Inlet velocity and boundary condition	0 $m \cdot s^{-1}$; velocity inlet
Outlet boundary condition	Pressure outlet
Initial velocity	0 $m \cdot s^{-1}$
Surface temperature of the hot casting	180 °C
Initial ambient temperature	25 °C
Total transient simulation time	15 s

Dust particles are tracked using the DPM model for Lagrangian trajectory tracking. The

particle size is described using the Rosin–Rammler function, with 5.263μm and 172.44μm as the lower and upper limits of the particle size distribution, respectively. The average particle size is taken as 31.64μm, the distribution width parameter is set The particle density is taken as 2600 kg/m³. The dust is continuously released from the surface of the sand drop platform as a surface source, with a mass flow rate set at 1.0×10^{-6} kg/s. The particle phase is calculated using one-way coupling, with its main parameters shown in Table 3.

Table 3. Discrete-phase model parameters

Discrete-phase parameter	Setting
Particle size distribution	Rosin–Rammler distribution
Minimum particle diameter	5.263μm
Maximum particle diameter	172.44μm
Mean particle diameter	31.64μm
Particle size distribution spread parameter	3.5
Particle size distribution spread parameter	10
Particle density	2600 $kg\cdot m^{-3}$
Particle release location	Surface of the shakeout platform
Particle release mode	Particle release mode
Particle mass flow rate	1.0×10^{-6} $kg\cdot s^{-1}$
Gas–particle coupling scheme	One-way coupling

In this setup, buoyancy caused by temperature differences is the main driving force for airflow within the computational domain. By performing transient coupled simulations of the temperature, velocity, and particle concentration fields, the model captures how shakeout dust

evolves over time and space, from its initial release near the source and upward movement to its subsequent deflection and dispersion.

4.Migration Patterns of Falling Sand Dust Under Thermal Plume Effects

Based on the numerical model and boundary conditions described above, transient simulations are conducted to examine shakeout-dust transport without mechanical supply or exhaust ventilation. This chapter first analyzes the development of the temperature, velocity, and dust concentration fields driven solely by thermal buoyancy. In this way, the basic dust-transport patterns can be identified without the influence of active ventilation.

The transient simulation covers a total period of 15 s. Four representative times—t = 1.0, 5.0, 9.0, and 12.0 s—are selected to represent the formation and development of the thermal plume, followed by the vertical transport, deflection, and dispersion of dust. By comparing the three fields at these times, the main transport pathways and spatial distribution of shakeout dust during thermal-plume development are identified..

4.1 Characteristics of Temperature Field Evolution Under Thermal Plume Action

The high-temperature casting and residual sand continuously transfer heat to the surrounding air, raising the air temperature near the heat source and forming thermal plumes under the influence of buoyancy due to temperature differences. To analyze the formation and development process of the thermal plume, the temperature fields of the XOZ and YOZ sections at t=1.0, 5.0, 9.0, and 12.0 seconds were compared, as shown in Fig. 8.

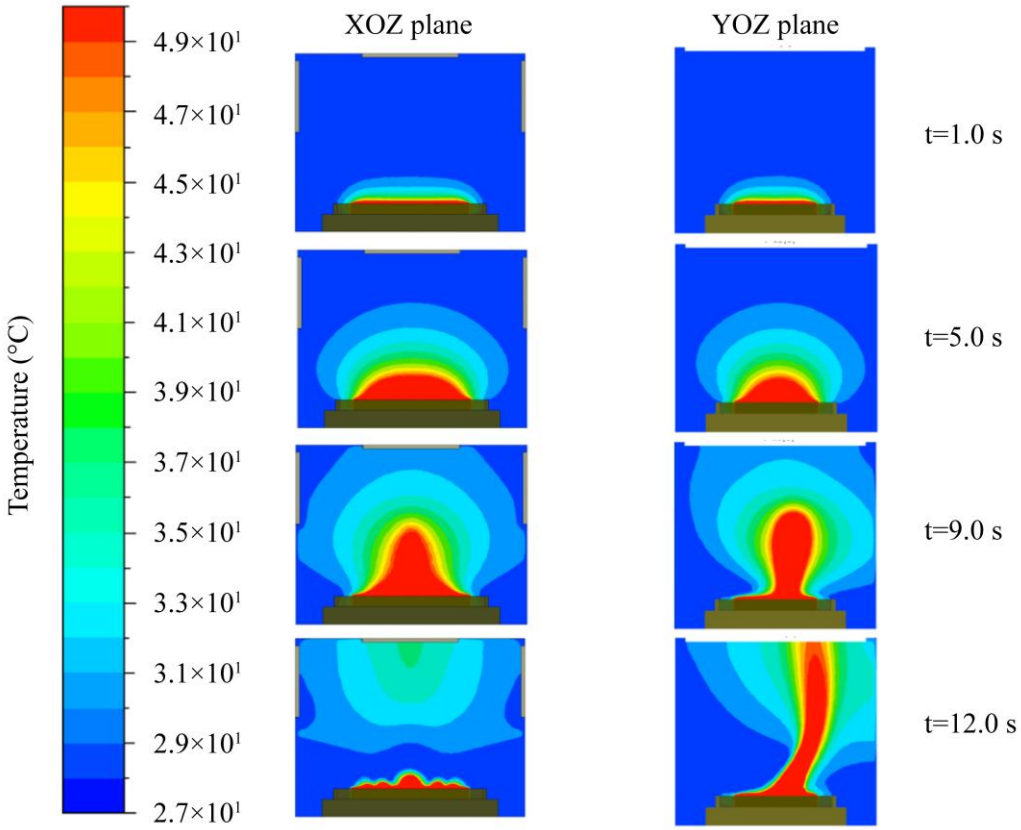


Fig. 8. Temperature field distribution at different times under the action of thermal buoyancy

It can be seen from Figure 8 that at t=1.0s, the temperature rise area in the two cross-sections is mainly distributed near the surface of the falling sand platform, in a thin layer or flat dome with a small range. The temperature change in other areas of the calculation domain is relatively small, indicating that the heat has not been obviously transferred to the upper part of the equipment, and the hot plume is in the initial formation stage. By t=5.0s, the temperature rise range in the XOZ cross-section and the YOZ cross-section is significantly expanded. The higher temperature area is still concentrated near the heat source, and its peripheral temperature equivalent line extends upwards to form a relatively complete dome structure. The temperature distribution of the two cross-sections at this moment is centered on the heat source, showing obvious symmetry as a whole, indicating that the heated air has begun to develop upwards, but the heat is still mainly concentrated in the lower part of the operation area.

When t=9.0s, the temperature field gradually changes from the early dome-like distribution to the plume structure extending vertically. The high-temperature area in the XOZ cross-section is located in the middle above the heat source, and the lower part is connected to the heat source, and the peripheral medium-temperature area extends upwards and to both sides. The high-temperature core in the YOZ cross-section is more concentrated, in a vertically elongated column shape, and a clear high-temperature transmission channel is formed above the heat source. Compared with t=5.0s, the vertical development characteristics of hot plume are more obvious at this time. By t=12.0s, there is a significant difference in the temperature distribution of the two cross-sections. In the XOZ cross-section, the higher temperature area has been extended to the upper part of the equipment, but the continuous high-temperature core has been weakened. Only the local high-temperature area is retained near the surface of the platform, and the upper space is mainly manifested as a large range of medium temperature rise area. In the YOZ cross-section, the high-temperature area still extends upwards continuously near the heat source, and obviously bends to the right side of the cross-section, forming an asymmetric high-temperature zone in the upper space. The results show that there is an obvious difference in direction in the later stage of thermal plume development, and its lateral deflection is more prominent in the YOZ cross-section.

Overall, in the sand drop operation area, the temperature field first forms a localized temperature rise near the surface of the heat source, then gradually expands into a dome-shaped structure, and further develops into a thermal plume extending in the vertical direction. As the simulation time increases, the morphology of the thermal plume in different cross-sections begins to show differences. In the later stages, the temperature rise zone in the XOZ section mainly

expands into the upper space, while the high-temperature core in the YOZ section exhibits a noticeable lateral bending. The aforementioned changes in the temperature field indicate that thermal buoyancy can drive heat from the vicinity of the sand settling platform to the upper part of the equipment, while the structure of the working space causes the thermal plume to exhibit an asymmetric distribution in the later stages of its development.

The aforementioned temperature contour analysis reflects the spatial distribution characteristics of the thermal plume within the computational domain but fails to accurately describe the variation of temperature along the vertical direction. Therefore, the geometric centerline on the YOZ plane was selected; temperature distribution data were extracted along the positive Z-axis—extending upward from the bottom of the sand-shakeout zone—at various simulation times, and temperature profile curves were plotted, as shown in Fig. 9.

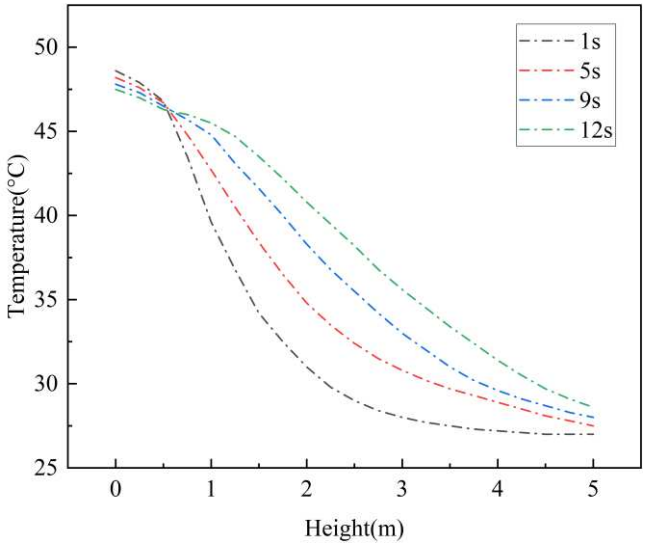


Fig. 9. Temperature profile curves at different simulation times along the centerline of the YOZ cross-section

As shown in Figure 9, the centerline temperature at different simulation times decreases with increasing height. However, as the simulation time extends, the temperature in the middle and upper regions gradually increases, and the thermal influence range continues to expand upward. At

1 second, the temperature at the bottom of the centerline is approximately 48.6 ℃; as the height increases, the temperature rapidly decreases, dropping to about 29.0 ℃ at Z=2.50 m, indicating that in the initial stage, the heat is mainly concentrated near the heat source, and the upper space is less affected by the heat.

When the simulation time increases to 5 seconds, the temperature change in the area near the heat source is small, while the temperature in the middle and upper regions increases somewhat. For example, the temperature at Z=1.50 m rises from 34.2℃ at 1 s to 38.4℃, an increase of 4.2℃; at Z=3.00 m, the temperature rises from 28.0℃ to 30.8℃. This result indicates that as the thermal plume gradually forms, heat begins to be transported from the near-source area to the upper part of the equipment. At 9 seconds, the centerline temperature curve continues to move toward higher temperatures, with the temperature at Z=2.00 m rising from 34.8℃ at 5 seconds to 38.3℃, an increase of 3.5℃; at Z=3.00 m, the temperature reaches approximately 33.0℃, indicating that the vertical influence range of the thermal plume has further expanded. By t = 12 s, the temperature near the source remains relatively stable, while temperatures in the middle and upper regions continue to increase.. For example, the temperature at Z=4.00 m reaches 31.4℃, an increase of about 4.2℃ compared to 1 s; the temperature at the bottom of the centerline slightly decreases from 48.6℃ to 47.5℃.

Overall, the temperature profile did not exhibit synchronous warming across the entire area, but rather showed a characteristic of small temperature changes near the source and gradually increasing temperatures in the middle and upper sections. This indicates that the thermal plume continuously transports heat from the sand-fall area to the upper part of the equipment, causing the temperature gradient along the height direction to gradually decrease and the thermal influence

range to continuously expand. This pattern of change is basically consistent with the cloud pattern characteristics of the high-temperature region developing in the vertical direction in Fig. 8.

4.2 Characteristics of Velocity Field Evolution under Thermal Plume Influence

The temperature difference between the high-temperature casting and the residual sand with the surrounding air causes the air near the heat source to rise, and promotes changes in the velocity field of the sand falling area over time. To analyze the flow field evolution characteristics during the formation and development of thermal plumes, the velocity fields at the XOZ and YOZ sections at t=1.0, 5.0, 9.0, and 12.0 seconds were compared, as shown in Fig. 10.

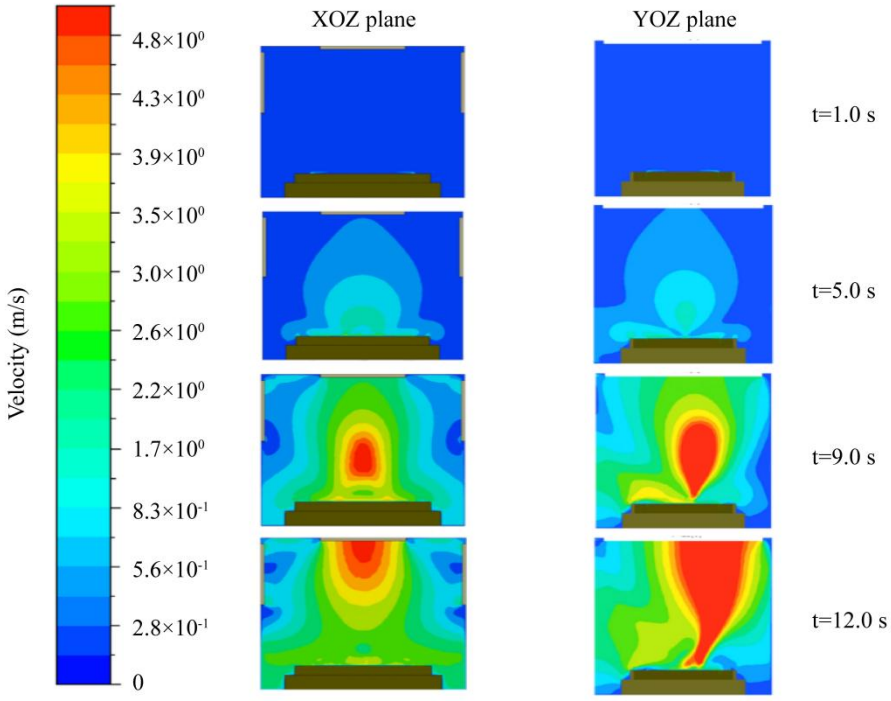


Fig. 10. Velocity field distribution at different times under the action of thermal buoyancy

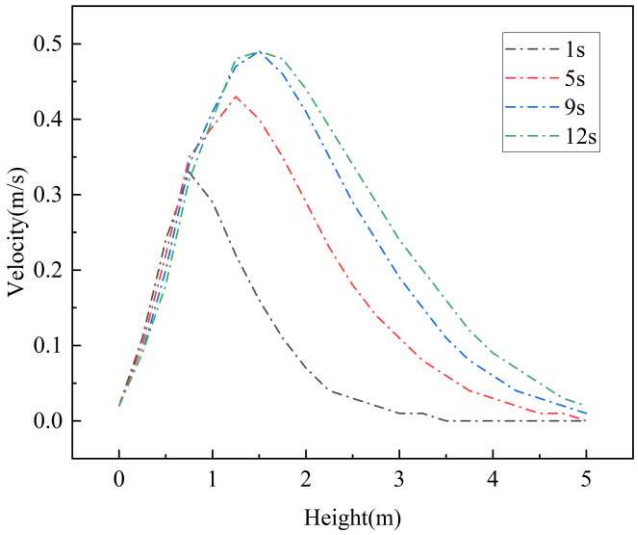
As shown in Figure 10, at t=1.0s, the airflow velocity within the two sections is generally low, and a clearly defined high-speed region has not yet formed, indicating that the driving effect of buoyancy due to temperature difference on the surrounding air is in its initial stage. By t=5.0s, a continuous high-speed region appears above the heat source, with its influence extending

vertically. The velocity distribution in the XOZ cross-section is relatively symmetrical, and the high-velocity region in the YOZ cross-section is also mainly located above the heat source. This change is consistent with the upward development of the high-temperature region described in Section 4.1, indicating that the thermal plume has formed. When t=9.0s, the airflow speed above the heat source significantly increases, with the high-speed area concentrated along the vertical direction. In the XOZ cross-section, the high-speed region is located in the middle above the heat source, while in the YOZ cross-section, a concentrated area extending upward from the vicinity of the heat source is formed, indicating that the vertical transport effect of the thermal plume is further enhanced. Compared to t=5.0s, the intensity and vertical influence range of the high-speed area have both increased at this time, and the main body of the thermal plume is clearer. By t=12.0s, the high-speed regions in both sections continue to expand toward the upper part of the equipment. In the XOZ section, the high-speed region remains primarily above the heat source, maintaining a central distribution characteristic overall. In the YOZ section, the high-speed region bends from near the heat source toward the right side of the section, forming a larger high-speed area in the upper space, exhibiting a clear It can be seen that the lateral deflection of the thermal plume in the later stages of its development exhibits certain sectional directional differences, with the deflection characteristics in the YOZ section being more pronounced.

Overall, the velocity field in the sand drop operation area has undergone a development process over time, transitioning from a low-speed state to the formation of a vertical high-speed zone, and then to the expansion in the upper space and local lateral deflection. The correspondence between the spatial distribution of the temperature field and the velocity field indicates that the temperature rise near the heat source is the main driving factor for the gradual enhancement of

603 airflow movement. After the formation of the thermal plume, the high-speed region mainly
604 develops above the heat source; as the thermal plume continues to rise, it exhibits lateral
605 deflection within the YOZ cross-section. This development of the flow field further influences the
606 upward transport of dust particles and their direction of dispersion in the upper space.

607 The velocity contours show the spatial extent of the thermal plume and the distribution of
608 high-velocity regions. However, they do not clearly quantify how the upward airflow changes
609 along the vertical direction. Therefore, the geometric centerline on the YOZ plane was selected.
610 Velocity distribution data were extracted along the positive Z-axis—extending upward from the
611 base of the sand-falling zone—at various simulation time points to plot velocity profile curves, as
612 shown in Fig. 11.



613

614 Fig. 11. Velocity profile curves at different simulation times along the centerline of the YOZ
615 cross-section

616 It can be seen from Fig. 11 that the centerline velocity at different simulation moments shows
617 a change law of increasing first and then decreasing with height, indicating that there is an obvious
618 plume acceleration area above the heat source. Unlike the temperature maximum value, which is
619 mainly located in the near-heat source area, the speed peak value appears within about 0.75-1.75

m from the falling sand area, reflecting the process of gradually accelerating the heated air under the buoyancy and the surrounding air coil absorption, and then slowing down due to the diffusion of plume and momentum dissipation. At 1 s, the peak speed is about 0.33 m/s, which appears around Z=0.75 m; then the speed decreases rapidly, and the speed in the area above Z=2.50 m is lower than 0.03 m/s, indicating that the rising airflow in the initial stage is mainly limited to the heat source. At 5 s, the speed peak increased to about 0.43 m/s and moved up to around Z=1.25 m. At the same time, the speed at Z=2.00 m increased from 0.07 m/s at 1 s to 0.29 m/s, and from 0.01 m/s to 0.11 m/s at Z=3.00 m, indicating that the vertical influence of hot plume has expanded significantly. At Z=0.50 m, the speed is slightly reduced from 0.24 m/s to 0.22 m/s, indicating that the flow field enhancement mainly occurs in the upper part of the equipment, and the speed increases synchronously in the area near the heat source. At 9 s, the speed peak is further increased to about 0.49 m/s, the peak position is around Z=1.50 m, and a high speed is maintained in the range of 1.25-1.75 m. Compared with 5 s, the speed at Z=1.50 m increased from 0.40 m/s to 0.49 m/s, and from 0.18 m/s to 0.29 m/s at Z=2.50 m, indicating that the vertical thickness and influence range of the high-speed area of plumes have increased. At 12 s, the peak speed is still about 0.49 m/s, and the peak position changes less, but the speed in the middle and upper regions continues to increase. For example, the speed at Z=2.50 m increased from 0.29 m/s at 9 s to 0.34 m/s, and from 0.11 m/s to 0.16 m/s at Z=3.50 m.

Overall, the development of the thermal plume is mainly characterized by the peak velocity moving upward from the near-source region, the gradual increase in peak velocity, and the expansion of the high-speed area toward the upper part of the equipment. From t = 9 to 12 s, the peak velocity remains relatively stable, while the airflow velocity in the middle and upper regions

continues to increase. This indicates that the main structure of the thermal plume is gradually taking shape. Its later development is mainly characterized by a continued upward expansion of the affected region.

4.3 Dust Migration Patterns Under Thermal Plume Influence

After the dust released from the surface of the sand drop platform enters the surrounding air, its migration process is influenced by the formation and development of thermal plumes. To analyze the spatiotemporal variation of the dust concentration field, the dust concentration distribution on the XOZ and YOZ sections at t=1.0, 5.0, 9.0, and 12.0 seconds was compared, as shown in Fig. 12.

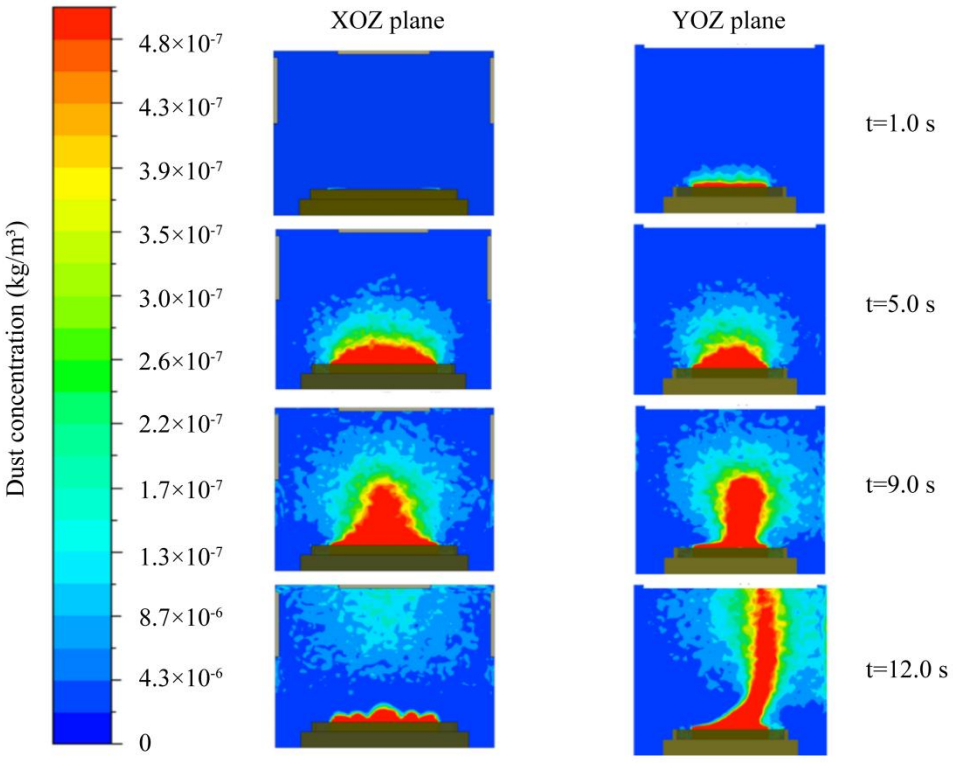


Fig. 12. Distribution of dust mass concentration at different times under the action of thermal buoyancy

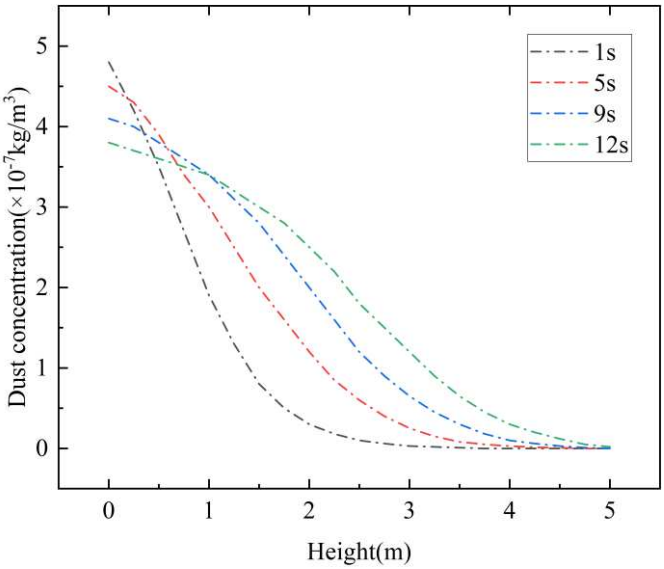
From Figure 12, it can be seen that at t=1.0s, the dust is mainly distributed near the surface of the sand drop platform, with both diffusion height and impact range being relatively small. In the

YOZ cross-section, a localized high-concentration area near the dust release surface can be observed, while in the XOZ cross-section, only a small range of near-source dust distribution appears, indicating that at this moment, the dust is still in the early release stage and has not formed a distinct By t=5.0s, the dust distribution range in both sections has expanded. The high-concentration area is still mainly located above the sand drop platform, with a surrounding region of medium to low concentration dust extending upwards, resembling a dome shape overall. The dust impact range in the XOZ section is relatively wide, while the high-concentration area in the YOZ section is more concentrated. A comparison of the temperature and velocity fields at the same time shows that a rising high-temperature region and a relatively high-velocity airflow region have formed above the heat source. As a result, the dust begins to move upward with the thermal plume. At t=9.0s, the high-concentration dust area extends upward from the vicinity of the sedimentation platform, forming a relatively continuous vertical distribution. In the XOZ cross-section, the upper part of the high-concentration area gradually narrows, with medium and low-concentration dust spreading to the sides; in the YOZ cross-section, the high-concentration core is more concentrated, taking on a vertically elongated cylindrical shape. At this moment, the high dust concentration area corresponds well in spatial position with the high-temperature core in Section 4.1 and the high-speed area in Section 4.2, indicating that the thermal plume has a significant entrainment and vertical transport effect on the dust. By t=12.0s, the dust concentration distribution in the two sections shows significant differences. In the XOZ section, there are still localized high-concentration dust areas near the surface of the sand drop platform, but their distribution no longer forms a continuous vertical high-concentration channel; a larger area of lower-concentration dust appears in the upper part of the equipment, indicating that the dust has

spread to In the YOZ cross-section, the high-concentration dust band still extends continuously upward from the release area and bends significantly to the right side of the cross-section, forming a directional asymmetric distribution at the upper part of the equipment. The direction of this deflection is consistent with the changes in the temperature field and velocity field at the same moment in the YOZ cross-section, indicating that the dust migration path is directly influenced by the later deflection of the thermal plume.

Overall, the falling sand dust under the influence of thermal plume exhibits distinct phased migration characteristics. In the early stages of the simulation, dust mainly accumulates near the release source; as the thermal plume forms, the dust gradually extends upward. After the thermal plume fully develops, a continuous vertical migration area of high-concentration dust forms above the heat source. In the later stages of the simulation, the dust The spatial correspondence between the temperature field, velocity field, and dust concentration field indicates that the upward airflow driven by thermal buoyancy is an important force for the vertical migration of dust, while the directional change of the thermal plume at the upper part of the equipment further affects the lateral diffusion path of the dust.

While dust concentration contour maps provide a visual representation of the spatial distribution of particles within the computational domain, they do not readily allow for a quantitative description of particle migration along the thermal plume. Therefore, the geometric centerline on the YOZ plane was selected; data on dust concentration distribution were extracted along the positive Z-axis—extending upward from the bottom of the sand-shakeout zone—at various simulation time points, and dust concentration profiles were plotted, as shown in Fig. 13.



699

700 Fig. 13. Profiles of dust concentration along the YOZ cross-section centerline at different

701 simulation times.

702 As shown in Figure 13, the centerline dust concentration at different simulation times

703 decreases with increasing height, indicating that the maximum dust concentration is always

704 located near the sedimentation area. However, as the simulation time is extended, the dust

705 concentration in the middle and upper regions gradually increases, and the rate of decrease in

706 concentration with height slows down, indicating that the influence range of the dust continues to

707 expand upward. At t = 1 s, the peak dust concentration is approximately 4.8×10-7 kg/m³ and

708 occurs near Z = 0 m. The concentration decreases rapidly with height, falling to about 8.0×10-8

709 kg/m³ at Z = 1.50 m. This distribution indicates that, during the initial stage, most dust remains

710 close to the release source because the thermal plume has not yet established a clear vertical

711 particle-transport pathway. By t = 5 s, the dust concentration near the source decreases slightly,

712 while concentrations in the middle and upper regions increase noticeably.. For example, the

713 concentration at Z=1.00 m increased from 1.9×10^{-7} kg/m³ at 1 s to 3.0×10^{-7} kg/m³, an increase of

714 approximately 57.9%; at Z=2.00 m, it increased from 3.0×10^{-8} kg/m³ to 1.2×10^{-7} kg/m³, an

715 increase of approximately 300%. This indicates that as the updraft gradually forms, some particles
716 begin to be transported from the near-source area to the center of the equipment. At 9 seconds, the
717 dust concentration curve further extends into the higher altitude region. Although the
718 concentration peak is still near the sedimentation area, the dust concentration within the range of
719 Z=1.00-3.00 m continues to increase. Among them, the concentration at Z=1.50 m reached
720 2.8×10^{-7} kg/m³, an increase of about 40% compared to 5 seconds; at Z=3.00 m, the concentration
721 reached approximately 6.5×10^{-8} kg/m³. This indicates that the thermal plume has been able to
722 transport more particles to the upper space of the equipment. By 12 seconds, the dust
723 concentration in the near-source area continued to slightly decrease, while the concentration in the
724 middle and upper areas maintained an increasing trend. For example, the concentration at Z=3.00
725 m increased from 3.0×10^{-9} kg/m³ at 1 second to 1.2×10^{-7} kg/m³, reaching about 40 times the initial
726 value; at Z=4.00 m, the concentration increased from nearly zero to approximately 3.0×10^{-8} kg/m³.
727 This result indicates that in the later stages of the simulation, the newly added particles did not
728 continue to concentrate near the release source, but instead moved more with the rising airflow
729 into the upper space of the equipment.

730 Overall, the peak dust concentration in the center line is always located in the near source
731 area, but the middle and upper dust concentration continues to increase over time, and the
732 concentration decay gradient gradually decreases. This shows that the development of thermal
733 plume increases the vertical transport altitude of dust, so that the dust distribution gradually
734 changes from near-source concentration to the middle and upper space along the rising air flow.
735 The change has a good spatial and temporal correspondence with the evolutionary characteristics
736 of the temperature field and velocity field.

4.4 Discussion

In this study, the temperature field, velocity field and dust concentration field showed a relatively consistent vertical development trend over time, but there are certain differences in the distribution characteristics of the three along the altitude direction. The highest temperature of the center line is always near the heat source, and the speed peak appears at a certain distance above the heat source. This is because the density of the air near the heat source decreases after being heated and moves upwards under the action of buoyancy. In the process of rising, the airflow continues to suck the surrounding air and gradually accelerates, so the maximum speed is not at the same height as the maximum temperature. After reaching the peak, the velocity of the center line gradually decreases with the lateral diffusion and momentum dissipation of the plume. The difference in the spatial position of the temperature peak and the speed peak reflects the evolutionary process of the thermal plume from the near source to the accelerated development to the upward diffusion.

There is an obvious time and space correspondence between the dust concentration profile and the development of hot plumer flow. In the early stage of the simulation, the ascending airflow has not been fully developed. The dust is mainly concentrated near the falling sand platform, and the concentration decreases rapidly with altitude. As the speed of the middle and upper regions increases, the dust concentration at the same altitude gradually increases, and the concentration decay deceleration rate decreases accordingly along the altitude direction. It should be noted that the peak dust concentration at different simulation moments is always near the release source and does not move up as a whole; the main function of the hot plume is to expand the vertical impact range of dust and continue to transport some particles to the upper space of the equipment.

759 Therefore, it is difficult to fully reflect the dust migration process based on the maximum
760 concentration position alone. It should also be judged in combination with the concentration
761 changes at different altitudes and the impact range of dust.

762 In the later stages of the simulation, the temperature field, velocity field, and dust
763 concentration field all exhibited an asymmetric characteristic of deflection to the right on the YOZ
764 section, while the distribution on the XOZ section was relatively symmetrical. Due to the absence
765 of other external airflow drives during the calculation process, this directional difference is mainly
766 related to the semi-enclosed spatial structure and boundary conditions of the sand drop equipment.
767 The enclosure structures on both sides of the equipment, as well as the openings at the top and
768 sides, restrict the free diffusion of the thermal plume and alter the local flow path at the upper part
769 of the equipment, causing the upward airflow and the dust particles it carries to deflect laterally
770 within the YOZ This indicates that the spatial distribution of the falling dust is not only influenced
771 by thermal buoyancy but is also closely related to the enclosure structure and the position of the
772 openings of the equipment.

773 From the perspective of dust control, the area near the sand drop platform remains the region
774 with the highest dust concentration and should be the focus of near-source dust control.
775 Meanwhile, the vertical migration area above the heat source and the lateral deflection area at the
776 top of the equipment may also form continuous dust transport and Therefore, the identification of
777 dust control areas should not be based solely on near-source concentrations, but should also
778 consider the vertical transport channels formed by the development of thermal plumes and their
779 directional changes at the top of the equipment. The results of this study can provide a theoretical
780 basis for the subsequent identification of key dust control areas at the sand drop station.

Based on the on-site layout shown in Fig. 2, the sand dropping station currently has exhaust vents on both sides, an exhaust vent on the top, and an air curtain. According to the dust migration patterns obtained in this paper, the area near the sand falling platform is a high-concentration near-source area, while the area above the heat source and the upper part of the equipment are the main areas for vertical transport and deflection diffusion of dust. Therefore, the on-site ventilation system should balance the near-source control near the sand settling platform and the collection of dust above the equipment, while also paying attention to the coordination between the left and right exhaust volumes and the air curtain with the exhaust airflow, to avoid airflow disturbances that could cause dust to spread to the Since this paper does not simulate the mechanical ventilation operating conditions, the actual control effect of the existing system still needs to be further evaluated in conjunction with on-site wind speed tests or numerical simulations of ventilation conditions.

In order to highlight the relationship between hot plume and dust migration under the action of temperature difference buoyancy, this paper appropriately simplifies the actual operation process on the basis of retaining key geometric features such as the main body of the sand dropper, the sand drop platform, the enclosure structure and the main opening. In the actual process of falling sand, the temperature of the casting and mold sand will decay with time, and the dust release also has obvious intermittent and non-uniformity. At the same time, factors such as mechanical vibration, sand block drop, equipment gaps, local environmental airflow, particle deposition and secondary dust may have an impact on the local airflow structure and dust distribution. In addition, dust particles have certain differences in shape, particle size and surface properties, and their actual movement behavior may be more complex than ideal spherical

803 particles. Therefore, the results obtained in this paper are mainly used to reveal the basic laws of
804 thermal plume formation, vertical development and dust migration under typical conditions. The
805 follow-up research can further introduce the heat source and dust release conditions that change
806 over time, and incorporate the actual operating parameters of the exhaust, top exhaust and jet air
807 curtain on the left and right sides of the site into the model, and carry out multi-factor coupling
808 analysis in combination with mechanical disturbance, particle deposition and local structure of the
809 equipment to evaluate the dust capture of the existing ventilation system. Set the matching
810 relationship between the effect and the air delivery and exhaust parameters.

811 ## 5 Conclusions

812 This paper combines on-site dust detection and numerical simulation to study the thermal
813 plume induced by temperature difference buoyancy in a semi-enclosed sand drop station under
814 non-mechanical ventilation conditions and its impact on dust migration. By analyzing the changes
815 in the temperature field, velocity field, and dust concentration field at different simulation times,
816 the following main conclusions are drawn:

817 (1) The total dust concentration around the sand drop machine is 8.0-11.0 mg/m³, with the
818 peak concentration at the operating position being 10.7 mg/m³ and the concentration at the
819 forward detection point in the work area being 9.2 mg/m³. This indicates a significant dust
820 pollution in the sand drop operation area, with certain concentration differences between different
821 detection locations.

822 (2) Under the conditions of a heat source surface temperature of 180 ℃ and an initial
823 ambient temperature of 25 ℃, the airflow above the heat source gradually develops from localized
824 buoyancy to a continuous vertical thermal plume. The centerline velocity exhibits a distribution

characteristic of first increasing and then decreasing with height, with the peak velocity rising from approximately 0.33 m/s at 1 second to about 0.49 m/s at 9 seconds, and the peak value remaining relatively constant at 12 seconds. Meanwhile, the velocity in the middle and upper regions continues to increase, indicating that the later stage of the thermal plume is primarily characterized by the high-speed region extending toward the upper part of the equipment.

(3) The peak dust concentration has always been near the falling sand platform, but with the development of hot plume, the dust concentration in the middle and upper regions gradually increases, the concentration decay deceleration rate along the altitude direction decreases, and the dust influence range continues to expand upwards. At 9 s, the dust forms a relatively continuous vertical distribution above the heat source; at 12 s, more particles enter the upper space of the equipment and show an asymmetric feature of deflecting to the right in the YOZ cross-section. Therefore, the near-source area near the falling sand platform, the vertical migration area above the heat source and the deflection diffusion area on the upper part of the equipment should be the focus of the coordinated control of the on-site ventilation and dust removal system.

References

[1]Siltanen E, KOPONEN M, Kokko A, et al. Dust exposure in Finnish foundries[J]. Scandinavian Journal of Work, Environment & Health, 1976: 19-31.

[2]Andersson L, Bryngelsson I L, Ohlson C G, et al. Quartz and dust exposure in Swedish iron foundries[J]. Journal of occupational and environmental hygiene, 2008, 6(1): 9-18.

[3]Tong R, Cheng M, Ma X, et al. Quantitative health risk assessment of inhalation exposure to automobile foundry dust[J]. Environmental geochemistry and health, 2019, 41(5): 2179-2193.

[4]Duan D, Leng P, Li X, et al. Characteristics and occupational risk assessment of occupational

847 silica-dust and noise exposure in ferrous metal foundries in Ningbo, China[J]. Frontiers in Public
848 Health, 2023, 11: 1049111.
849 [5]Li Q, Li X, Qin G, et al. Application and comparison of five risk assessment methods in ferrous
850 metal foundry enterprises with silica dust concentration exceeding the limit posts[J]. Frontiers in
851 Public Health, 2025, 13: 1465284.
852 [6]Gong X, Xiao X, Zhao J, et al. Influence of particle size on the separation performance and
853 flotation kinetics of foundry dust[J]. Process Safety and Environmental Protection, 2024, 183:
854 178-187.
855 [7]Cai Y, Yan B, Zhang C, et al. Dust transport and diffusion under individual and coupled dust
856 source conditions in a fully mechanized coal mining face[J]. Granular Matter, 2026, 28(2): 41.
857 [8]Huo S, Liu C, Ma W, et al. Numerical simulation study on the influence of shearer mining
858 intensity on dust distribution characteristics[J]. Process Safety and Environmental Protection,
859 2025, 202: 107684.
860 [9]Xue S, Zhang W, Tu Q, et al. Dynamic model construction and particle size effects analysis of
861 dust movement during coal-cutting operations at mining face[J]. Powder Technology, 2025, 460:
862 121058.
863 [10]Li Y, Chen X, Du Y, et al. Research on the Distribution Law of Air Flow and Dust in Multi-
864 Process Operations of Coal Mine Fully Mechanized Caving Face[J]. Energy Science &
865 Engineering, 2025, 13(11): 5247-5267.
866 [11]Tian D, Wu X, Yao J, et al. Study on Dust Distribution Law in Open-Pit Coal Mines Based on
867 Depth Variation[J]. Atmosphere, 2025, 16(7): 771.
868 [12]Zhou W, Cui Y, Wang H, et al. Study on the characteristics of dust diffusion during a truck

869 travelling in an open-pit coal mine affected by the vertical wind shear[J]. Journal of Hazardous
870 Materials, 2025, 483: 136611.
871 [13]Wang Z, Yan J, Zhou W, et al. WRF-FLUENT Coupled Modeling Approach for Simulating
872 Airflow and Dust Dispersion during Cold Periods in Cold-Region Open-Pit Mines[J]. Journal of
873 Hazardous Materials, 2026: 141242.
874 [14]Wang J, Luo Z, Zhang G, et al. Experimental and numerical simulation of road dust
875 distribution and transport characteristics under disturbance of automobile tire in open-pit mine[J].
876 Journal of Wind Engineering and Industrial Aerodynamics, 2025, 266: 106214.
877 [15]Tang S, Wei C, Zhang W, et al. A Review of Dust Movement Laws and Numerical
878 Simulation-Based Dust Suppression Methods in Coal Mines[J]. Processes, 2026, 14(6): 928.
879 [16]An J, Geng F, Feng Y, et al. Mechanism-based assessment of respirable dust exposure in
880 miners: Integrating CFD-DPM simulation with personalized monitoring for occupational health
881 risk[J]. Journal of Environmental Chemical Engineering, 2026: 122551.
882 [17]Yu H, Xie Y, Yang X, et al. Migration and deposition characteristics of micro-dust in the
883 human upper airway in dust-polluted tunnel environments[J]. Journal of Hazardous Materials,
884 2025, 488: 137371.

885 Data Availability

886 All data generated during the numerical simulations in this study are included in this article and its
887 supplementary information files.

888 Acknowledgements

889 This study was supported by the Open Research Fund of the NHC Key Laboratory for
890 Engineering Control of Dust Hazard (No. KLECDH2025020101). The funders had no role in

study design, data collection and analysis, decision to publish, or preparation of the manuscript.

Author contributions

JWC : Funding Acquisition and Conceptualization. XYW.: Writing - Original Draft Preparation. FQC : Writing - Review & Editing and Project Administration. YL : Software. FBZ : Investigation. JJL : Validation. GYL : Data Curation.

Competing interests

The authors declare no conflicts of interest.